Oxygen Transport Ceramic Membranes

Quarterly Report

October 2005 – December 2005

Principal Authors:

Prof. S. Bandopadhyay

Dr. T. Nithyanantham

Issued: February 2005

DOE Award # DE-FC26-99FT40054

University of Alaska Fairbanks
Fairbanks, AK 99775

Contributing sub contractors:

1. **X.-D Zhou, Y-W. Sin and H. U. Anderson,** Materials Research Center, University of Missouri-Rolla, Rolla, MO 65401
2. **Prof. Alan Jacobson and Prof. C.A. Mims;** University of Houston/University of Toronto

DISCLAIMER

ABSTRACT

The present quarterly report describes some of the investigations on the structural properties of dense OTM bars provided by Praxair and studies on newer composition of Ti doped LSF.

The *in situ* electrical conductivity and Seebeck coefficient measurements were made on LSFT at 1000 and 1200^{o}C over the oxygen activity range from air to 10^{-15} atm. The electrical conductivity measurements exhibited a p to n type transition at an oxygen activity of $1x10^{-10}$ at 1000^{o}C and $1x10^{-6}$ at 1200^{o}C. Thermogravimetric studies were also carried out over the same oxygen activities and temperatures. Based on the results of these measurements, the chemical and mechanical stability range of LSFT were determined and defect structure was established.

The studies on the fracture toughness of the LSFT and dual phase membranes exposed to air and N_2 at 1000°C was done and the XRD and SEM analysis of the specimens were carried out to understand the structural and microstructural changes. The membranes that are exposed to high temperatures at an inert and a reactive atmosphere undergo many structural and chemical changes which affect the mechanical properties. A complete transformation of fracture behavior was observed in the N_2 treated LSFT samples.

Further results to investigate the origin of the slow kinetics on reduction of ferrites have been obtained. The slow kinetics appear to be related to a non-equilibrium reduction pathway that initially results in the formation of iron particles. At long times, equilibrium can be reestablished with recovery of the perovskite phase.

Recent results on transient kinetic data are presented. The 2-D modeling of oxygen movement has been undertaken in order to fit isotope data. The model is used to study “frozen” profiles in patterned or composite membranes.

TABLE OF CONTENTS

LIST OF GRAPHICAL MATERIALS

INTRODUCTION

Conversion of natural gas to liquid fuels and chemicals is a major goal for the Nation as it enters the 21st Century. Technically robust and economically viable processes are needed to capture the value of the vast reserves of natural gas on Alaska's North Slope, and wean the Nation from dependence on foreign petroleum sources. Technologies that are emerging to fulfill this need are all based syngas as an intermediate. Syngas (a mixture of hydrogen and carbon monoxide) is a fundamental building block from which chemicals and fuels can be derived. Lower cost syngas translates directly into more cost-competitive fuels and chemicals.

The currently practiced commercial technology for making syngas is either steam methane reforming (SMR) or a two-step process involving cryogenic oxygen separation followed by natural gas partial oxidation (POX). These high-energy, capital-intensive processes do not always produce syngas at a cost that makes its derivatives competitive with current petroleum-based fuels and chemicals.

In the mid 80's BP invented a radically new technology concept that will have a major economic and energy efficiency impact on the conversion of natural gas to liquid fuels, hydrogen, and chemicals.[1] This technology, called Electropox, integrates oxygen separation with the oxidation and steam reforming of natural gas into a single process to produce syngas with an economic advantage of 30 to 50 percent over conventional technologies.[2]

The Electropox process uses novel and proprietary solid metal oxide ceramic oxygen transport membranes [OTMs], which selectively conduct both oxide ions and electrons through their lattice structure at elevated temperatures.[3] Under the influence of an oxygen partial pressure gradient, oxygen ions move through the dense, nonporous membrane lattice at high rates with 100 percent selectivity. Transported oxygen reacts with natural gas on the fuel side of the ceramic membrane in the presence of a catalyst to produce syngas.

---

[1]Mazanec, T. J.; Cable, T. L.; Frye, J. G., Jr.; US 4,793,904, 27 Dec **1988**, assigned to The Standard Oil Company (now BP America), Mazanec, T. J.; Cable, T. L.; US 4,802,958, 7 Feb **1989**, assigned to the Standard Oil Co. (now BP America), Cable, T. L.; Mazanec, T. J.; Frye, J. G., Jr.; European Patent Application 0399833, 24 May **1990**, published 28 November **1990.**

[2]Bredesen, R.; Sogge, J.; "A Technical and Economic Assessment of Membrane Reactors for Hydrogen and Syngas Production" presented at Seminar on the Ecol. Applic. of Innovative Membrane Technology in the Chemical Industry", Cetraro, Calabria, Italy, 1-4 May **1996**.

[3] Mazanec, T.J., *Interface*, **1996**; Mazanec, T.J., *Solid State Ionics*, 70/71, **1994** 11-19; "Electropox: BP's Novel Oxidation Technology", T.J. Mazanec, pp 212-225, in "The Role of Oxygen in Improving Chemical Processes", M. Fetizon and W.J. Thomas, eds, Royal Society of Chemistry, London, **1993**; "Electropox: BP's Novel Oxidation Technology", T.J. Mazanec, pp 85-96, in "The Activation of Dioxygen and Homogeneous Catalytic Oxidation", D.H.R. Barton, A. E. Martell, D.T. Sawyer, eds, Plenum Press, New York, **1993**; "Electrocatalytic Cells for Chemical Reaction", T.J. Mazanec, T.L. Cable, J.G. Frye, Jr.; Prep Petrol Div ACS, San Fran, **1992** *37*, 135-146; T.J. Mazanec, T.L. Cable, J.G. Frye, Jr.; *Solid State Ionics*, **1992**, 53-56, 111-118.

In 1997 BP entered into an OTM Alliance with Praxair, Amoco, Statoil and Sasol to advance the Electropox technology in an industrially sponsored development program. These five companies have been joined by Phillips Petroleum and now are carrying out a multi-year $40+ million program to develop and commercialize the technology. The program targets materials, manufacturing and engineering development issues and culminates in the operation of semi-works and demonstration scale prototype units.

The Electropox process represents a truly revolutionary technology for conversion of natural gas to synthesis gas not only because it combines the three separate unit operations of oxygen separation, methane oxidation and methane steam reforming into a single step, but also because it employs a chemically active ceramic material in a fundamentally new way. On numerous fronts the commercialization of Electropox demands solutions to problems that have never before been accomplished. Basic problems in materials and catalysts, membrane fabrication, model development, and reactor engineering all need solutions to achieve commercial success. Six important issues have been selected as needing understanding on a fundamental level at which the applied Alliance program cannot achieve the breadth and depth of understanding needed for rapid advancement. These issues include:

1. Oxygen diffusion kinetics (University of Houston);
2. Phase stability and stress development (University of Missouri - Rolla);
3. Mechanical property evaluation in thermal and chemical stress fields (University of Alaska Fairbanks)

Statement of Work

Task 1 *Evaluate phase stability and thermal expansion of candidate perovskite membranes and develop techniques to support these materials on porous metal structures.*

Task 2 *Determine materials mechanical properties under conditions of high temperatures and reactive atmospheres.*

Task 3 *Measure kinetics of oxygen uptake and transport in ceramic membrane materials under commercially relevant conditions using isotope labeling techniques.*

EXECUTIVE SUMMARY

Research on the Oxygen Transport Membranes as identified in tasks 1-3 are being performed at the various universities under the stewardship of Praxair. The quarterly technical report presents the progress of the tasks defined to understand the fundamental concepts and structural performance of the OTM material.

LSFT is a p-type semiconductor in the higher oxygen activity regime, but becomes n-type as the oxygen activity decreases with the p-type to n-type transition occurring at oxygen activities of $1x10^{-10}$ atm and $1x10^{-6}$ atm for temperatures of 1000°C and at 1200°C, respectively. The magnitude of the electrical conductivity and position of the p to n transition is determined by both the relative concentrations of the electronic carriers as well as the oxygen vacancy concentration. According to the TGA study, the weight decreased continuously until dissociation occurred at 10^{-15} atm. Upon reoxidation, the weight loss was found to be reversible, eventhough, dissociation had occurred and the electrical conductivity had changed from p to n type. . This is a very good sign since LSFT not only exhibits higher conductivity (n-type) in the low oxygen activity regime, but also has a higher concentration of oxygen vacancies which improves the performance as an oxygen permeable membrane.

The LSFT and dual phase membranes were heat treated at 1000°C for 60min and air and N_2 atmosphere. The XRD and SEM analysis of the specimens were carried out to understand the structural and microstructural changes. The membranes that are exposed to high temperatures at an inert and a reactive atmosphere undergo many structural and chemical changes which affect the mechanical properties. A complete transformation of fracture behavior was observed in the N_2 treated LSFT samples.

We have continued to investigate the thermodynamic properties (stability and phase-separation behavior) and total conductivity of prototype membrane materials. The data are needed together with the kinetic information to develop a complete model for the membrane transport. We have previously reported characterization, stoichiometry, conductivity, and dilatometry measurements for several perovskite compositions. In this period, we have investigated the origin of the very slow kinetics in the intermediate pressure range for ferrites. A model for the non-equilibrium has been developed.

The combination of gradientless measurements with isotope investigations under steady state, provide a complete picture of the performance of OTM materials. In the case of the $La_{0.2}Sr_{0.8}Fe_{0.8}Cr_{0.2}O_{3-x}$ membrane here, the irregular structural changes observed in these materials are implicated in the large variation in observed surface rates.

Task 1: Preparation and Characterization of Dense Ceramic oxygen Permeable Membranes

Yong-Wook Sin and H. U. Anderson[1]

Materials Research Center, University of Missouri-Rolla, Rolla, MO 65401

Conductivity and Seebeck coefficient of $La_{0.2}Sr_{0.8}Fe_{0.55}Ti_{0.45}O_{3-\delta}$ (LSFT) as a function of temperature

Experimental

$La_{0.2}Sr_{0.8}Fe_{0.55}Ti_{0.45}O_{3-\delta}$ (LSFT) powder was fabricated using the glycine-nitrate combustion synthesis process and calcined at 600°C for 2 hours to minimize the remaining organics. Powders were isostatically pressed into a pellet under the pressure of 217 MPa followed by sintering at 1400°C for 5 hours. A rectangular bar (2.2 mm x 3.3 mm x 20 mm) was prepared from the pellet for the conductivity and Seebeck coefficient measurements. Five gm of LSFT powder was also prepared to measure weight changes as a function of oxygen activity and temperature by TGA.

Results and Discussion

The test procedure used was to first measure the electrical conductivity at a given temperature in air and then to re-measure the electrical conductivity at a series of decreasing oxygen activities which were established by the CO/CO_2 ratio in a flowing gas mixture. After a series of measurements was completed in the reducing direction, the reversibility was checked by again measuring the electrical conductivity at a series of increasing oxygen activities with the end point being air. All the data points were collected only after the sample was fully stabilized at a given atmosphere at both 1000 and 1200°C.

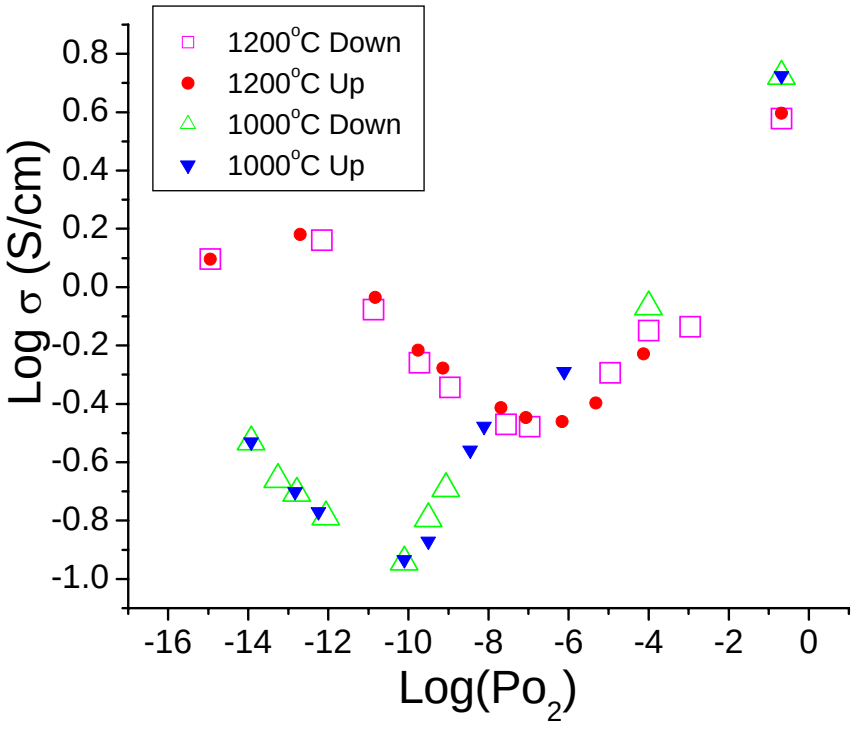

Figure 1. Electrical conductivity as a function of oxygen activity of LSFT at 1000 and 1200°C

The results of the electrical conductivity measurements of LSFT are shown in Figure 1. As can be seen, LSFT is a p-type semiconductor in the higher oxygen activity regime, but becomes n-type as the oxygen activity decreases with the p-type to n-type transition occurring at oxygen activities of $1x10^{-10}$ atm and $1x10^{-6}$ atm for temperatures of 1000°C and at 1200°C, respectively. The magnitude of the electrical conductivity and position of the p to n transition is determined by both the relative concentrations of the electronic carriers as well as the oxygen vacancy concentration. For example, observe in Figure 1, the whole plot including the minimum point (the electrical conductivity at the p-type to n-type transition) was shifted to higher oxygen activity range when the temperature was increased from 1000 to 1200°C. In addition, the conductivity at 1200°C is higher than the conductivity at 1000°C for oxygen activity below $1x10^{-8}$ atm , however when the oxygen activity exceeds $1x10^{-8}$ atm, the conductivity at 1000°C is larger than that at 1200°C. This phenomenon is because in the p type conduction region, $p = [Sr'_{La}] - 2[V^{\bullet\bullet}_{O}]$. Since the concentration of oxygen vacancies, $[V^{\bullet\bullet}_{O}]$, is higher at 1200°C than at 1000°C, the electrical conductivity of LSFT at 1200°C is lower in the p-type regime because the holes

which result from the acceptor concentration, $[Sr'_{La}]$, are compensated by the oxygen vacancies. As the oxygen activity continues to be decreased, the n-type conductivity regime is entered when sufficient oxygen vacancies have been generated to totally compensate the acceptors. At this point, the conductivity starts to increase with further decreases in oxygen activity with a negative pressure and exponential temperature dependency. This results in the n-type conductivity at 1200 ^{o}C being higher than that observed for 1000^{o}C. The increase of $[V^{\bullet\bullet}_{O}]$ in the n-type regime was verified by the TGA study (shown in Figure 2).

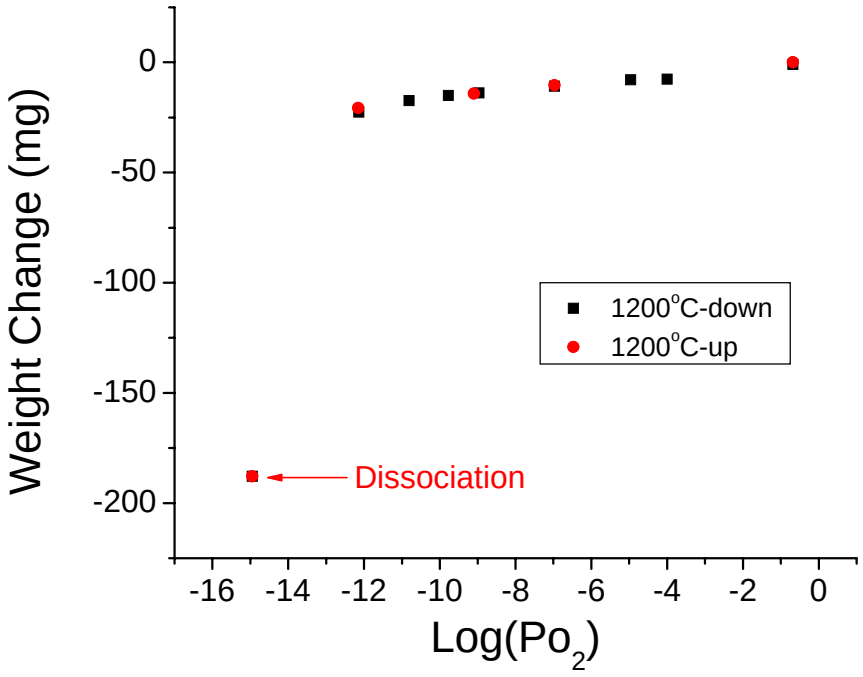

Figure 2. TGA of LSFT as a function of oxygen activity at 1200^{o}C

According to the TGA study, the weight decreased continuously until dissociation occurred at 10^{-15} atm. Upon reoxidation, the weight loss was found to be reversible, eventhough, dissociation had occurred and the electrical conductivity had changed from p to n type. . This is a very good sign since LSFT not only exhibits higher conductivity (n-type) in the low oxygen activity regime, but also has a higher concentration of oxygen vacancies which improves the performance as an oxygen permeable membrane. The crystal structure and microstructure of LSFT will be investigated using XRD and SEM to confirm this observation

The future work will be (1) to find out optimum composition of LSFT to maximize performance by increasing the concentration of oxygen vacancies and electrical conductivity and (2) to find out the temperature and oxygen activity limit for the chemical and mechanical stability of LSFT.

The Seebeck coefficient was also measured as a function of oxygen activity in air at 1000 and 1200°C (Figure 3 and 4). As can be seen, the Seebeck coefficient indicated p-type conductivity in the high oxygen activity regime and n-type conductivity in the lower oxygen activity regime. The electrical conductivity measurement of LSFT exhibited its p-type to n-type transition at about $1x10^{-10}$ atm of oxygen activity at 1000°C and $1x10^{-6}$ atm at 1200°C. However, the Seebeck coefficient showed its p-type to n-type transition at $1x10^{-8}$ atm at 1000°C and $1x10^{-6}$ atm at 1200°C. The difference between the two measurements occurs because of differences in the carrier mobilities. These differences will be will be investigated in the future.

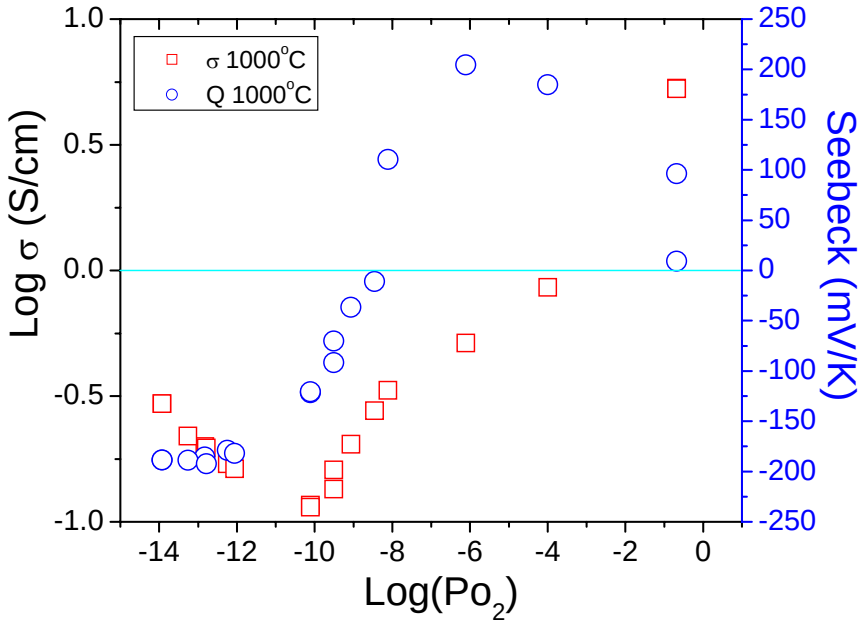

Figure 3. Electrical conductivity and Seebeck coefficient as a function of oxygen activity of LSFT at 1000°C

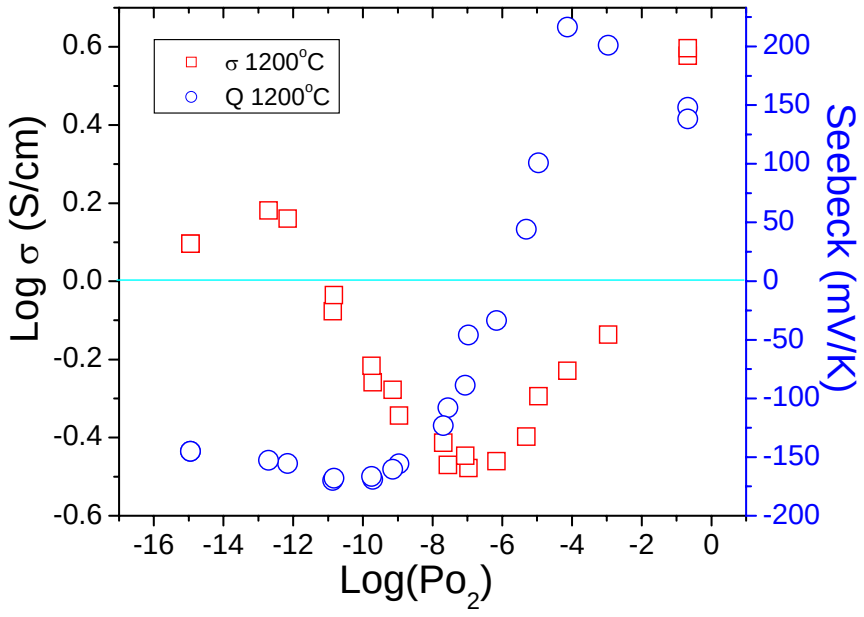

Figure 4. Electrical conductivity and Seebeck coefficient as a function of oxygen activity of LSFT at 1200°C

Future studies

1. The TGA measurement will be carried out as function of oxygen activity and temperature to find out the optimum composition of LSFT to maximize performance by increasing the concentration of oxygen vacancy and electrical conductivity
2. The chemical and mechanical stability limit of LSFT will be investigated.
3. XRD and SEM study will be carried out to confirm the full recovery of LSFT after dissociation.

TASK 2: Determine material mechanical properties under conditions of high temperature and reactive atmosphere

Prof. S. Bandopadhyay and Dr. T. Nithyanantham
University of Alaska Fairbanks, AK 99775

Experimental:

The LSFT and LSFT-CGO (dual phase) membranes were cut into small pieces and polished using polishing sheets and diamond pastes. The final polishing was carried out using 1μm diamond paste and the polished samples were used for heat treatment in the air and N_2 atmosphere. The temperature for the heat treatment was chosen as 1000°C and the air and N_2 (200ml/min) was chosen as the atmospheres. The samples were heated at the rate of 20°C/ min and dwelled at the maximum temperature for 60 min prior to cooling to room temperature. The Vicker's indentation method was used to analyze the hardness and fracture toughness of the membrane. Four loads (100, 300, 500 and 1000g) were used for performing indentation and 10 and 30 seconds were used as two loading times at each load. The fracture toughness of the membranes was calculated using the equations of Niihara et al. (1982). Crack lengths were measured from the optical micrographs of the indentations and cracks.

Results and Discussion:

Fracture Toughness of the LSFT and dual phase membranes:

The fracture toughness values of the membranes are shown in Figure 5. Two important observations from can be made from the figure.

1. In both (LSFT and dual phase) the membranes the fracture toughness value increases with increasing load. This trend was not affected by the heat-environment treatment of the specimens.
2. The fracture toughness value of the LSFT exposed to N_2 is lesser than the LSFT exposed to air at 1000°C. This behavior can be observed in all test loads. Also it is evident that the fracture toughness of the "as received" LSFT has not changed at the maximum test load even it was exposed to air at 1000°C.

The change in the fracture behavior of the membranes due to the heat treatment in N_2 atmosphere is mainly due to the changes occurred in the microstructure or in the crystal structure. The change in the hardness (Figure 6) and L/a values (Figure 7) of the LSFT membranes heat treated in the

air and N_2 environment in the test loads show that the samples exposed to N_2 favors an extensive crack growth.

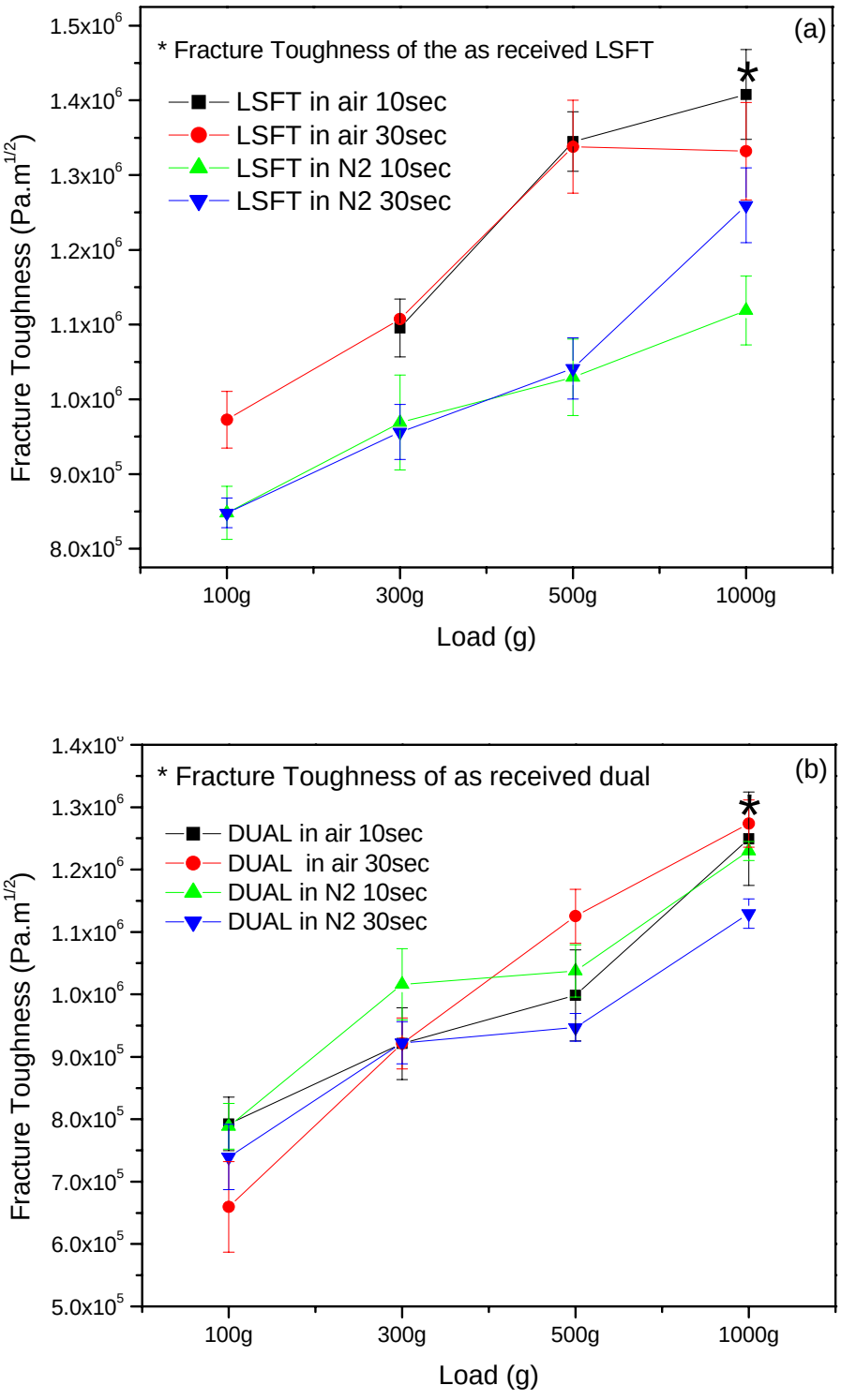

Figure 5. Fracture toughness of the LSFT and dual phase membranes

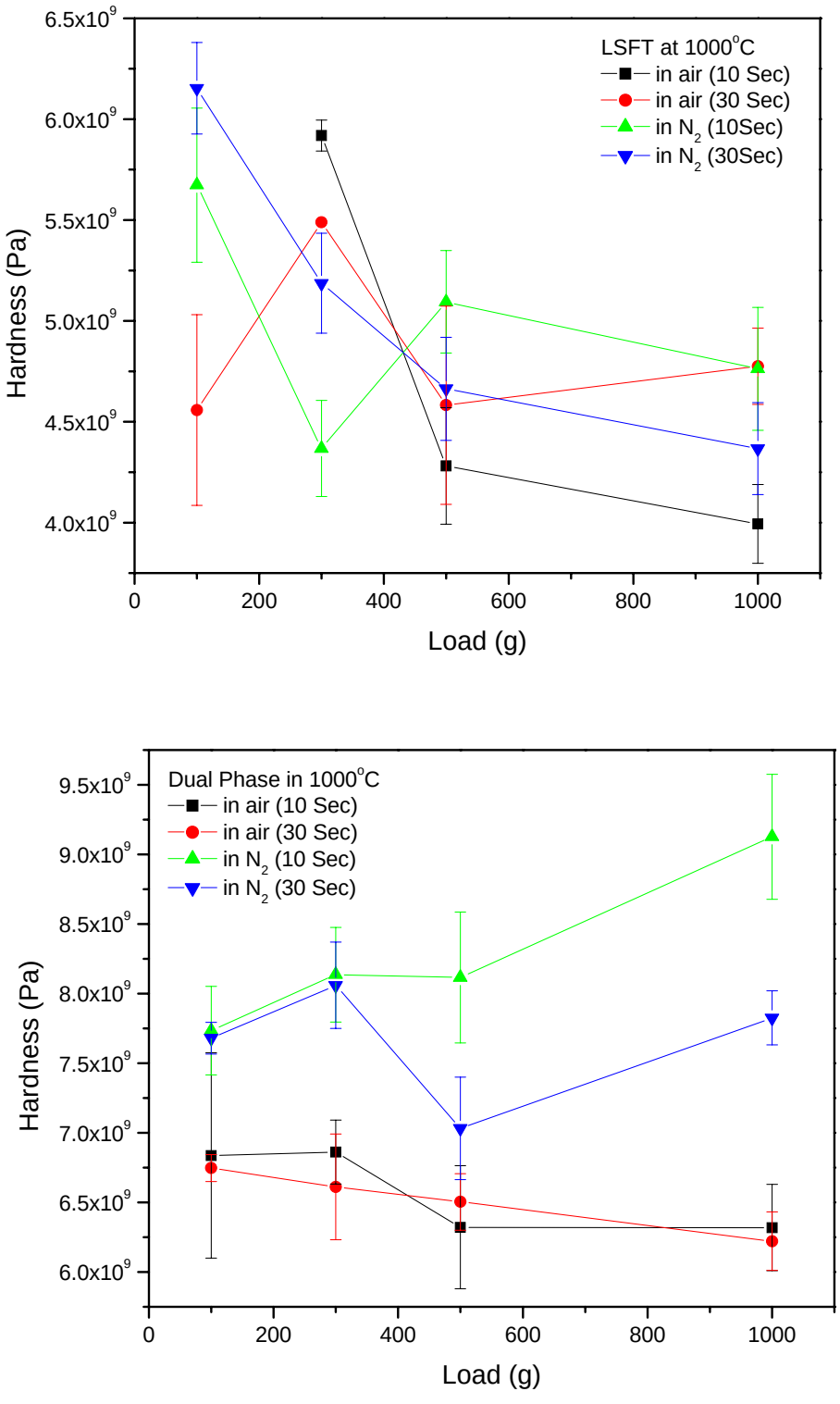

Figure 6. Hardness of the LSFT and dual phase membranes

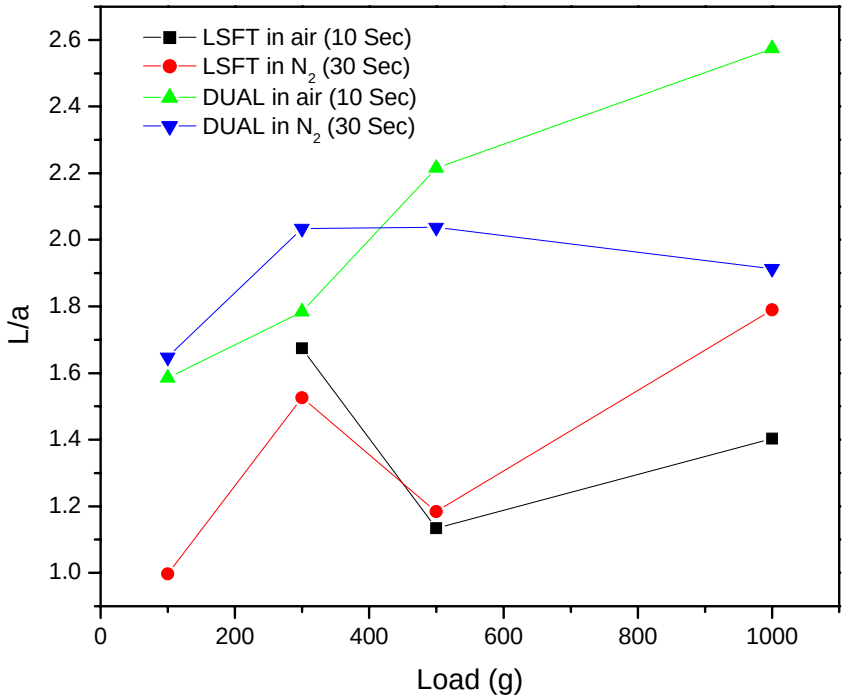

Figure 7. Dependence of L/a of LSFT and dual phase membranes on indentation load.

Figure 7 confirms the effect of environment on the crack propagation in the membranes. The L/a of the N_2 exposed samples are higher in most of the test loads than the samples exposed to air. The increase in L/a means the crack generated at a given load is longer as the hardness values are slightly higher than the samples exposed to air. The structural changes occurred in the samples due to the N_2 atmosphere might have altered the elastic/plastic properties of the membrane. The energy given during the indentation process was mostly used for the generation new surfaces rather than the plastic deformation of the membrane. In order to understand the fracture behavior in the heat treated samples, the fractured surfaces of the membranes were analyzed using SEM.

The SEM micrographs of the as received LSFT are shown in the Figure 8. The fracture is predominantly transgranular in nature and the pores are distributed evenly along the fractured plane. This shows the crack growth has not occurred through the grain boundaries and hence it is clear the grain boundaries have no weaker bonds or interactions.

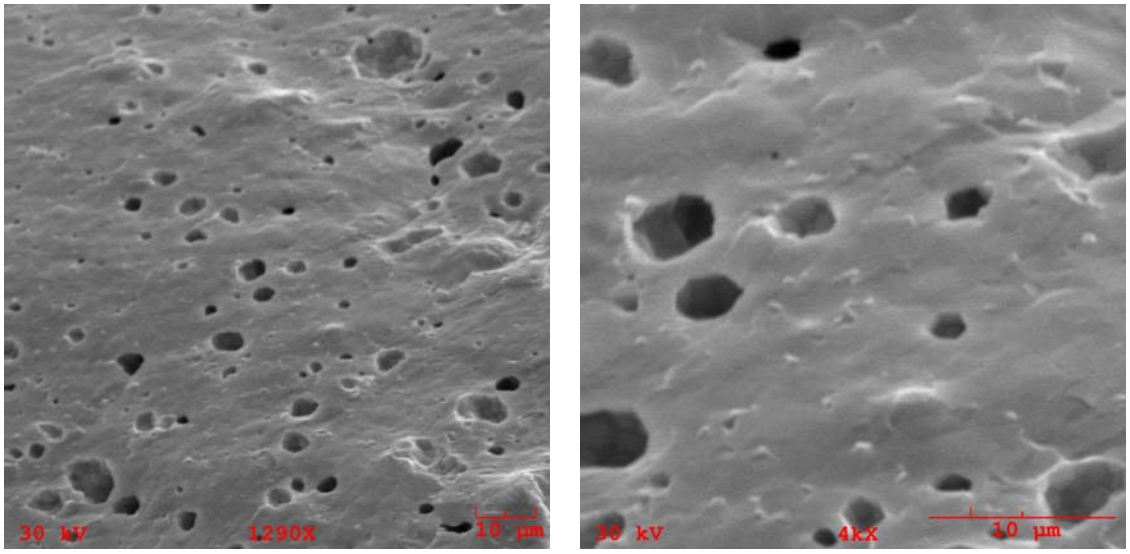

Figure 8. SEM micrographs of the as received LSFT. The fracture surface shows a transgranular fracture behavior.

The fracture surfaces of the heat treated LSFT in air and N_2 environment are shown in the Figure 9. The fracture surfaces of the LSFT exposed to air show a transgranular fracture as the tendency for an intergranular fracture can also be observed in some places. This may be due to the weakening of the grain boundaries as a result of high temperature treatment in air. The effect of N_2 on the fracture behavior is very much evident from the micrographs. The fracture is clearly intergranular and not even a trace of transgranular fracture is observed from the micrograph. The transformation in the fracture behavior is significant and the closer observation of the fracture surface shows large grain pull outs and the absence of any grain boundary precipitates. There is no significant grain growth in the N_2 exposed LSFT and this intergranular fracture behavior is mainly facilitated by structural changes happened due to the N2 atmosphere.

The x-ray diffraction analysis was carried out for the LSFT and dual phase membranes. The "as received" and heat treated samples were powdered and the analysis was carried out. The refinement of the XRD data was carried out and the results are summarized in Table 1. The x-ray diffraction patterns are shown in Figure 10. The crystal structure was found to be orthorhombic. Interestingly, samples tested under environment (N_2) shows some shift in the higher angles (Figure 10). However, further refinement of the data will be done considering the changes in the crystal structure.

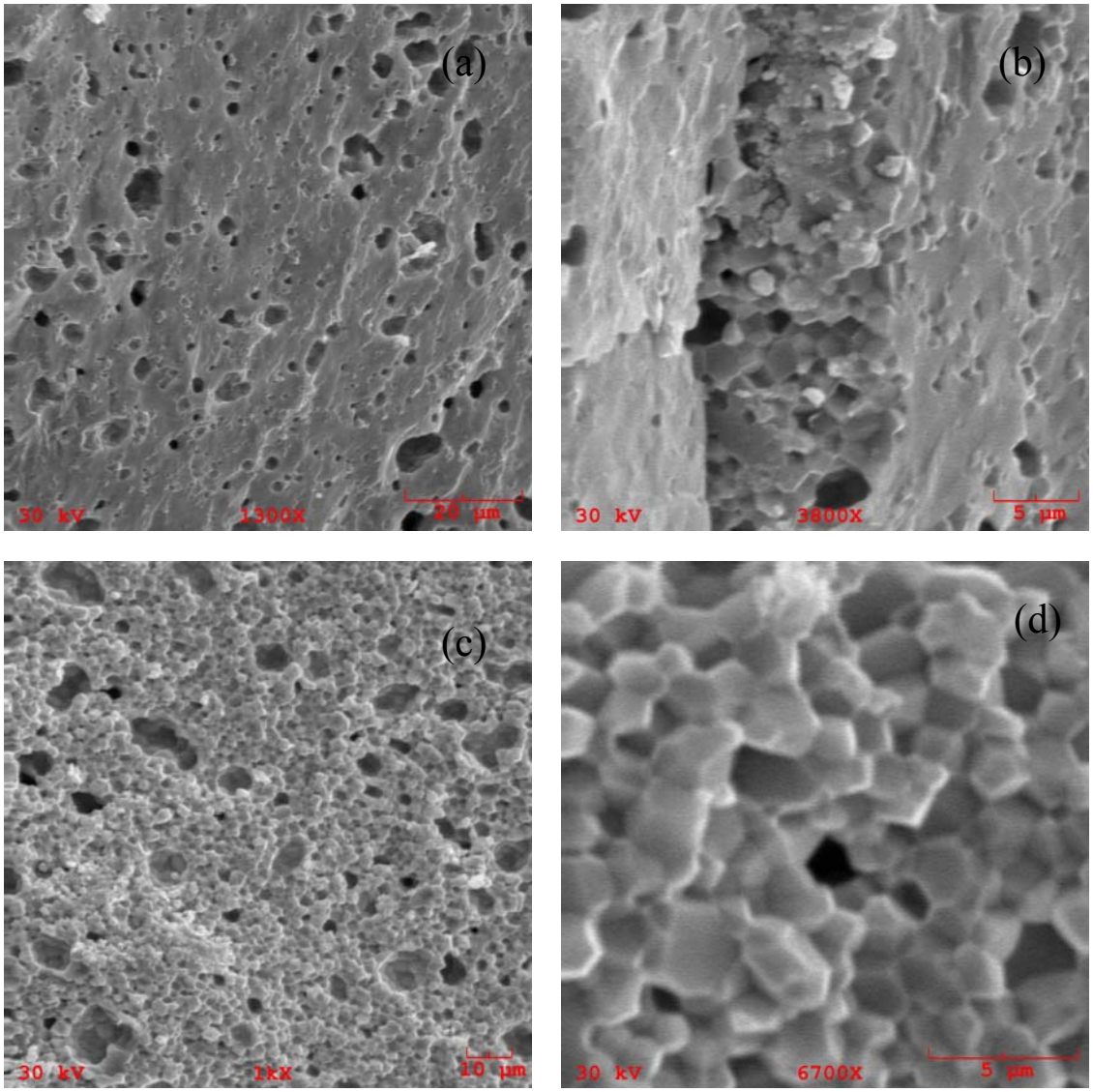

Figure 9. SEM micrographs of the LSFT membrane exposed to air (a & b) and N_2 (c & d) at 1000°C.

Table 1. Lattice parameters obtained from refinement of XRD data

Condition	**Crystal Structure**	**a**	**b**	**c**	**α=β=γ**
LSFT-as received	Orthorhombic	3.92	3.908	3.92	90
LSFT- exposed to Air, 1000°C	Orthorhombic	3.92	3.908	3.92	90
LSFT- exposed to N_2, 1000°C	Orthorhombic	3.92	3.908	3.92	90

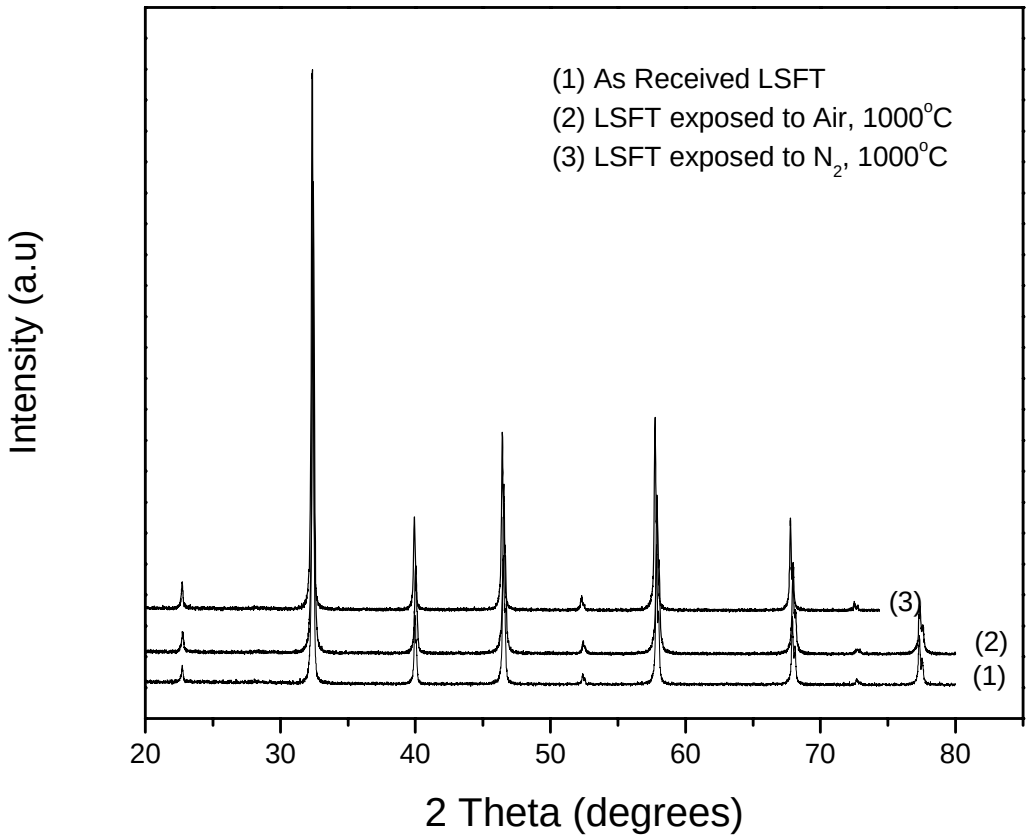

Figure 10. XRD plots of the LSFT membranes.

The dual phase (LSFT-CGO) membranes were also exposed to air and N_2 at 1000°C characterized by SEM and XRD in order to understand the fracture behavior of the membrane upon the exposure to the environments. Dependence of fracture toughness of dual phase membranes on indentation load is shown in Figure 5. Figure 6 shows the dependence of L/a of dual phase membranes on indentation load. Even though, there was no significant change in the fracture toughness of the dual phase membrane due to the environment, there was a noticeable change in the L/a values with the increasing load. The SEM micrograph of the phase membranes are shown in the Figure 10. The microstructure of the dual phase membrane is composed of a continues porous phase and a dense phase. The dense phase is surrounded by the porous microstructure. The microstructures of the as received membrane (a & b) show the microstructural inhomogeneities i.e the presence of continuous porous phase and the isolated dense. On the contrary to the dense phase, the fracture behavior of the porous phse is mainly intergranular.

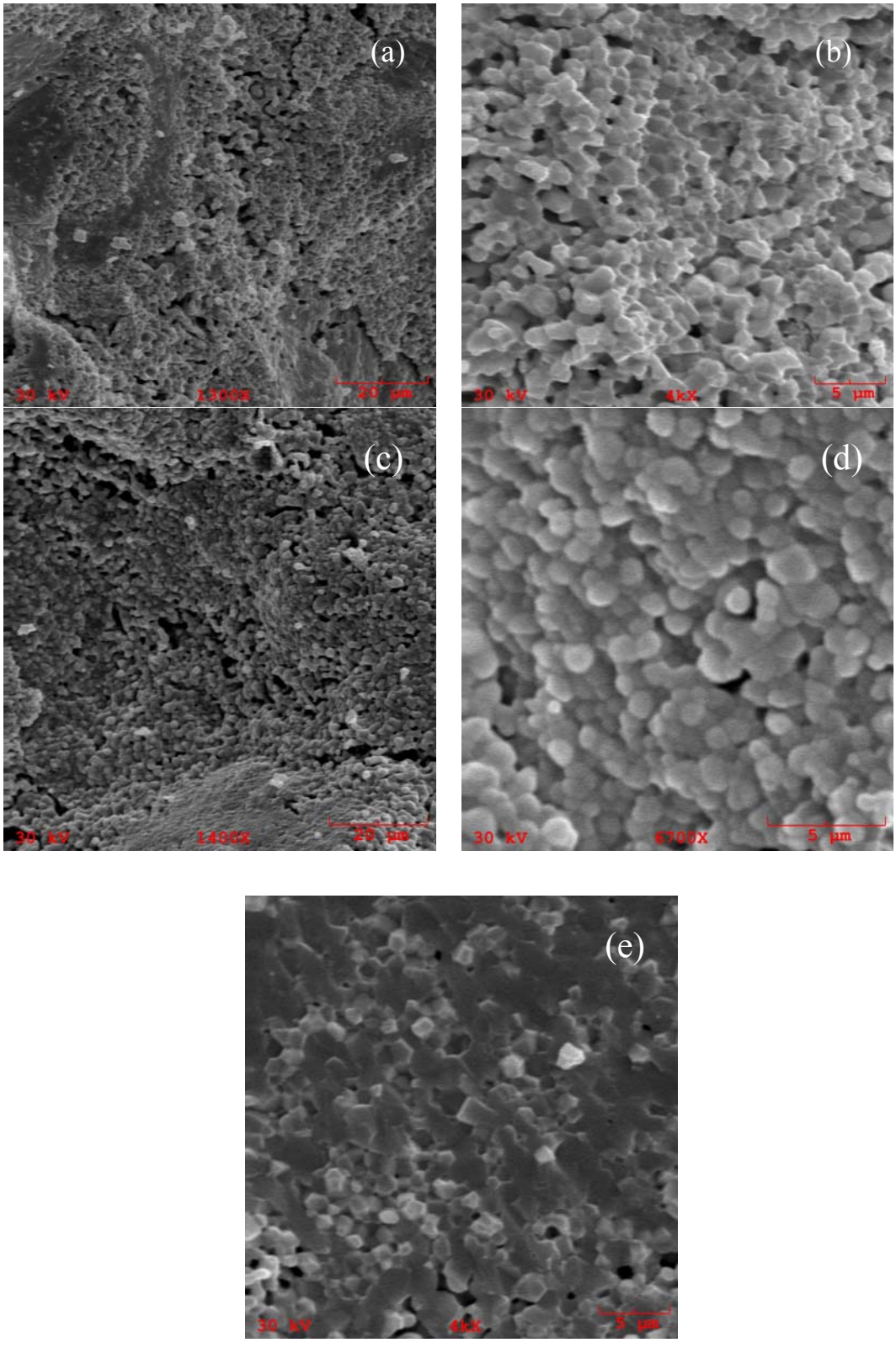

Figure 10. SEM micrographs of the dual phase membranes: as received (a & b), exposed to air (c, d & e) at 1000°C.

The fracture surface of the dual phase membrane which was exposed to air too reveals the presence of both the phases (Figure 10c) and the closer observation of the porous and dense regions are shown in Figure 10d and 10e. Even though the fracture in the porous region appears to be intergranular the fractured grains are mostly spherical and cleaved at the boundaries. The fracture at the dense region is mainly transgranular and some grain pull outs are observed in some places.

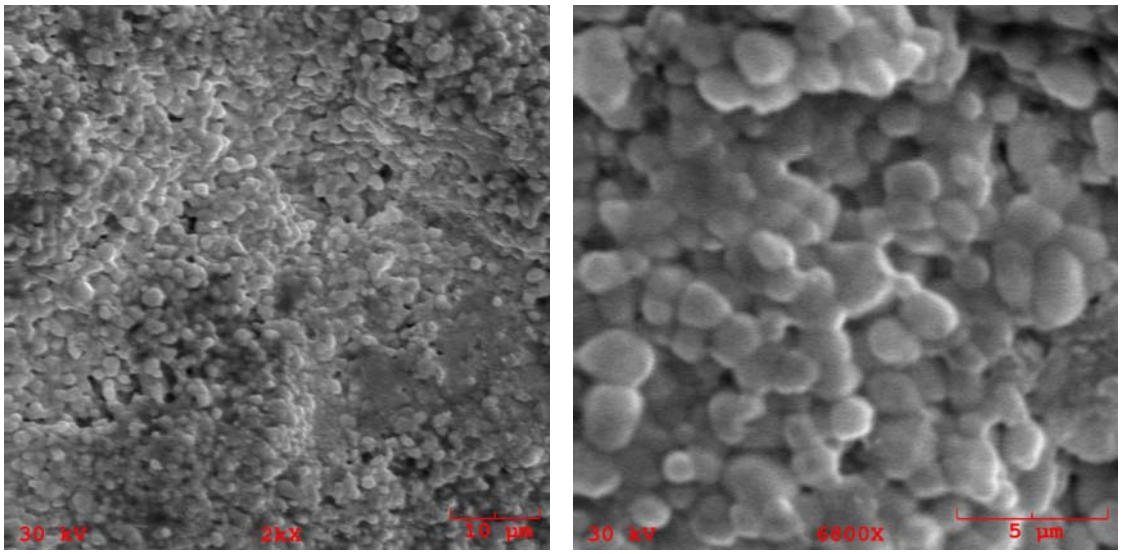

Figure 11. SEM micrographs of the dual phase membranes exposed to air at 1000°C.

Figure 11 shows the fracture surfaces of the dual phase membranes which are exposed to air at 1000°C. The presence of the dense phase along with the continuous porous phase is observed and the closer observation of the porous region shows a noticeable grain growth. The change in the grain size has not affected the fracture toughness of the membrane significantly and it is reported in Figure 5b.

The x-ray diffraction analysis of the as received and heat treated membranes are shown in the Figure 12. The crystalline phases were identified and marked. An orthorhombic LSFT and cubic CGO are the two identified crystalline phases. A clear shift in the peaks of the N_2 exposed samples is observed. Although, this suggests the phase instability and a possible decomposition of the parent structure upon exposure to the N_2 environment and high temperature, the possibility of the structural change needs to be examined. Hence, complete thermal analysis and refinement of the XRD data will be helpful to understand the structural changes associated with the exposure to the N_2 environment.

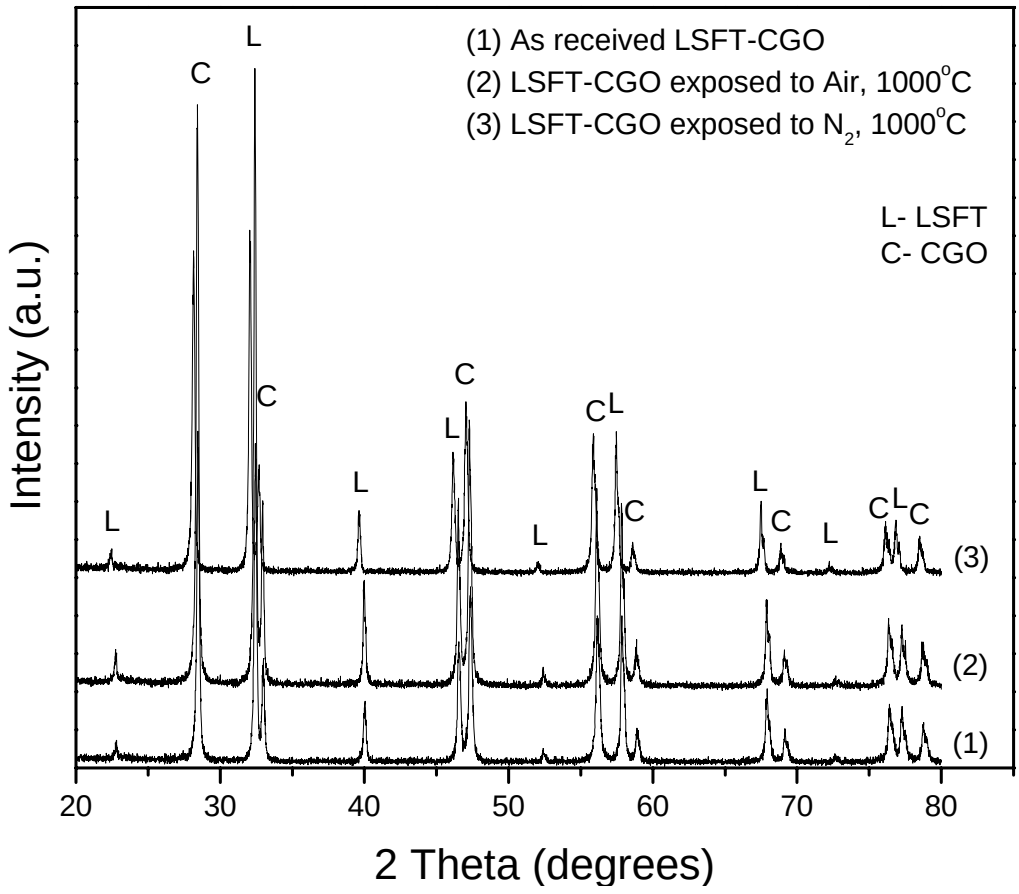

Figure 12. XRD plots of the dual phase membranes.

Plans for next quarter:

- Thermal analysis of the membranes at various environments.
- Refinement of the XRD data for the dual phase membranes
- Preparing samples for the flexural 4-point bend strength studies and doing fracture toughness studies at temperatures ranging from 300 to 1000 with various test loads.
- Room temperature flexural strength analysis.

Task 3: Measurement of Surface Activation/Reaction Rates in Ion Transport Membranes using Isotope Tracer and Transient Kinetic Techniques

A. J. Jacobson, University of Houston, C.A. Mims, University of Toronto

Introduction

Mixed ionic electronic conductors (MIECs) with the ABO_3 perovskite or related structures have been widely studied because of their practical applications in ion-transport membranes, pressure-driven oxygen generators, partial oxidation reactors, and as electrodes for solid oxide fuel cells (SOFCs) [1] A number of materials problems remain outstanding for the application of ion transport membrane reactors in the high oxygen partial pressure gradients found, for example, in *syn gas* generation by partial oxidation of methane. The membrane composition must simultaneously provide the necessary oxygen flux and have stability over a wide pO_2 range and appropriate mechanical properties.

The $La_{1-x}Sr_xFeO_{3-x}$ (LSFO) series has high mixed conductivity and better stability than the $La_{1-x}Sr_xCoO_{3-x}$ (LSCO) series but still exhibits limited stability in low-pO_2 environments. Additional substitution on the B-site by metal ions that are more difficult to reduce solves some of these problems but issues remain concerning both kinetic and thermodynamic stability and the effects of composition changes that result from partial decomposition or surface segregation on the membrane surface catalytic properties.

In our studies of membrane materials, we have investigated the pO_2 and temperature dependence of the conductivity, non-stoichiometry and thermal-expansion behavior of two specific compositions, $La_{0.2}Sr_{0.8}Fe_{0.8}Cr_{0.2}O_{3-x}$ and $La_{0.2}Sr_{0.8}Fe_{0.55}Ti_{0.45}O_{3-x}$, by using electrochemical cells and dilatometry [1,3,4,5]. Additional measurements on the simpler composition, $La_{0.5}Sr_{0.5}FeO_{3-x}$ have been made for comparison [1]. These and other recent studies of ferrites with the perovskite structure show anomalous behavior at low oxygen partial pressures ($<10^{-5}$ atm). The anomalies are due to non-equilibrium effects and can be avoided by using very strict criteria for the attainment of equilibrium. The slowness of the oxygen equilibration kinetics and the observation that deviations between equilibrium and non-equilibrium behavior become larger with increasing temperature suggest that cation rearrangements or phase separation must take place. The microscopic details of the mechanism responsible for the slow kinetics are not yet fully understood. In this paper, we present evidence that the slow kinetics are associated with

nanoscopic phase separation and suggest a general model that provides a basis for further experiments.

The large chemical gradients in operating oxygen transport membranes bring all of the structural issues above into play. Since variations in the structure and transport properties at any location in the membrane can have a large influence on the entire membrane, it is thus important to evaluate the membrane transport properties under an operating gradient. We have accomplished this by applying a transient isotopic tracing technique to an operating membrane. The evolution of the isotopic transient through the membrane following a pulse of $^{18}O_2$ to the "air" side reveals the surface activation parameters, their degree of reversibility, and the bulk transport properties in the presence of a large chemical gradient. These results reveal very different values from those obtained under gradientless conditions, suggesting that some of the complex features of the materials crystal structure play an important role in the membrane performance.

Experimental

Powders of $La_{0.2}Sr_{0.8}Fe_{0.55}Ti_{0.45}O_{3-x}$ and $La_{0.2}Sr_{0.8}Fe_{0.8}Cr_{0.2}O_{3-x}$, synthesized by using the spray pyrolysis method, were obtained from Praxair Specialty Ceramics (Woodinville, WA). The $La_{0.5}Sr_{0.5}FeO_{3-x}$ sample was synthesized by a self-propagating high temperature synthesis (SHS) method [6]. Electrical conductivity measurements were made in sealed electrochemical cells as a function of pO_2 at temperatures from 750 °C to 1000 °C down to 10^{-18} atm for the lowest temperatures. The measurements were made using an AC 4-point technique at a single frequency (1 kHz) and the phase angle monitored to confirm the absence of any polarization effects. Stoichiometry measurements were made in similar sealed electrochemical cells. The details of the sample characterization, conductivity and stoichiometry were reported previously [2-4]. Rectangular sample bars of $La_{0.2}Sr_{0.8}Fe_{0.55}Ti_{0.45}O_{3-x}$ sintered at 1450 °C were used for dilatometry measurements (NETZSCH, DIL 402C).[5] The chemical expansion data were obtained by switching the gas from air to pure argon or by using mixed gases (5% H_2/N_2, CO_2, and argon) in the temperature range between 800 and 1000 °C. The oxygen partial pressure (pO_2) was measured with an oxygen analyzer (AMETEK, TM-1B) at the outlet of the dilatometer.

For micro-structural studies, $La_{0.2}Sr_{0.8}Fe_{0.55}Ti_{0.45}O_{3-x}$ discs were quenched in air from 900 °C and different partial oxygen pressures (pO_2 = ~ 1.3×10^{-4}, 1.1×10^{-7}, 1.2×10^{-10}, 6.7×10^{-14} atm).

For comparison, $La_{0.5}Sr_{0.5}FeO_{3-\delta}$ discs were reduced at 950 °C for 24 ~ 48h in 5% H_2/N_2. Structural studies of quenched and reduced samples were performed by X-ray powder diffraction measurements with CuK_α radiation. Powder diffraction patterns of the samples were obtained in 0.01° steps with a preset count time of 5/sec, over the range $10° \leq 2\theta \leq 100°$.

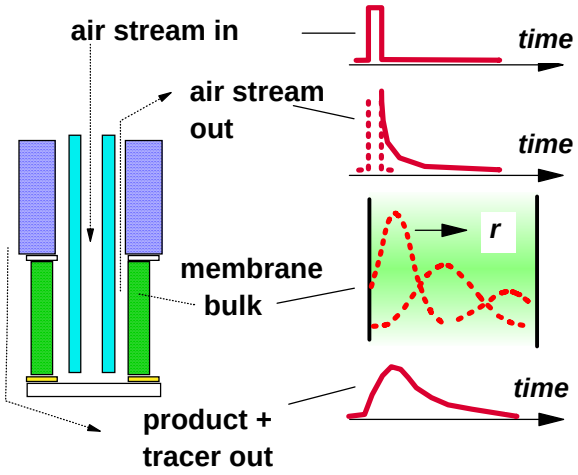

Figure 13. Membrane reactor and isotope transient experiment: left side shows reactor flow and sealing arrangement, right side shows conceptual ^{18}O isotope transient (from the top) of (1) the delivered isotope pulse, (2) the isotope decay transient in the air-side (the dashed line shows the tracer, solid line shows the ^{18}O decay arising from back exchange with the solid), (3) the ^{18}O wave evolution across membrane bulk and (4) ^{18}O delivered to product gas CO and/or CO_2.

Dense tubes of $La_{0.2}Sr_{0.8}Fe_{0.8}Cr_{0.2}O_{3-x}$ for membrane studies were formed by isostatic pressing followed by sintering. The two ends were cut and polished to provide parallel surfaces for sealing in the membrane reactor. The final fired dimensions were 6.0 mm o.d., 4.3 mm i.d by 12.0 mm long. A very slight non-concentricity resulted in a wall thickness of 0.85 ± 0.05 mm. The membrane was incorporated into a reactor assembly shown schematically in Figure 13. Briefly, the membrane was sealed by gold washers to a quartz air tube on top and a quartz disc on bottom. A re-entrant tube allows for positive air flow to the (inner) air side while an outer tube confines an annular down-flow to the syngas side gas. Constant sealing pressure is applied along the membrane axis. Both gas streams can be analyzed at the inlet or outlet by on-line gas chromatography or mass spectrometry. Isotope transients ($^{16}O_2$-$^{18}O_2$) were performed on a tubular (6 mm o.d., 0.85 mm wall) membrane of $La_{0.2}Sr_{0.8}Fe_{0.8}Cr_{0.2}O_{3-x}$ operating at steady state at

temperatures between 1023 K and 1173 K. A single high-gradient condition was established with synthetic "air" (20%O_2 : Ar) on one side and a CO:CO_2 mixture on the other. Figure 13 also shows an illustration of the isotope transient experiment. After achieving steady flux conditions, the oxygen on the air side was switched to $^{18}O_2$ (99%, Isotec) in a "pulse" while maintaining a constant pO_2 and flow rate. The resulting isotope transients are measured by on-line mass spectrometry, both on the air side as well as on the delivery "syngas" side. A one-dimensional (radial) model was used to simultaneously fit all of the experimental data from a given experiment. The total oxygen flux is given by the difference between the forward and reverse surface rates at each surface, and the back exchange of ^{18}O into the air side gas after the isotopic pulse provides a measure of the reversibility of oxygen activation. The bulk oxide ion diffusivity affects the shape of the transient observed on the syngas side. The best-fit kinetics parameters were determined by stochastic model runs. In a final experiment, the membrane was quenched during a repeat isotope transient and the internal ^{18}O distribution in the membrane was measured by imaging time-of-flight secondary ion mass spectroscopy (ToFSIMS – 25 keV Ga^+ primary ions) on polished cross-sections of the quenched membrane. The internal distribution can reveal internal variations in the oxygen diffusivity at steady state which cannot be resolved by the isotopic transients in the gas phases. Pressures < 10^{-9} mbar were maintained during ToFSIMS analysis to avoid surface oxygen exchange with background gases.

Results and Discussion

Non-equilibrium behavior

We have continued to investigate the thermodynamic properties (stability and phase-separation behavior) and total conductivity of prototype membrane materials. Most of the work this quarter has been in organizing our previous data into a form suitable for publication. The general observations are recapitulated in this report with some additional results and interpretation.

Slow kinetics observed in conductivity measurements:

The electrical conductivity data $La_{0.2}Sr_{0.8}Fe_{0.55}Ti_{0.45}O_{3-x}$ at 850 °C is shown in Figure 2 as a typical example. The measurements were made on both decreasing and increasing pO_2 using two different criteria for equilibrium. The conductivity data represented by the open and closed square symbols were obtained when the conductivity change was ≤ 0.0002 $Scm^{-1}min^{-1}$ and when the difference between the values of pO_2 measured by the pump and sensor cells differed by less than a half and order of magnitude at all pO_2 regions. Under these conditions the data taken on

increasing and decreasing pO2 agree suggesting that equilibrium was achieved. These data are compared with the results (open circles) obtained using an equilibrium criterion of ≤ 0.0005 $Scm^{-1}min^{-1}$. A difference between the measured values of pO_2 by the sensor and pump cells of more than one order of magnitude pO_2 was found under these conditions. The pO_2 differences between sensor and pump are slow to converge due to the slow kinetics and consequently both conductivity and pO_2 difference criteria are needed to ensure that equilibrium is reached.

The most striking feature of the comparison between the two experiments is the large difference in the conductivity in the range between $10^{-12} \leq pO_2 \leq 10^{-5}$ atm indicating that the reduction kinetics are very slow in this region. Similar slow equilibration kinetics have been observed in other ferrite perovskites including $SrFeO_{3-x}$ [1], $La_{1-x}Sr_xFeO_{3-y}$ [6,1,2,3], $La_{0.2}Sr_{0.8}Fe_{0.8}Cr_{0.2}O_{3-x}$ [2, 3] $LaSr_2Fe_{3-y}Cr_yO_{8+x}$ [1], and Ti-substituted $La_{1-x}Sr_xFeO_{3-y}$ (x = 0.5-0.7) [1]

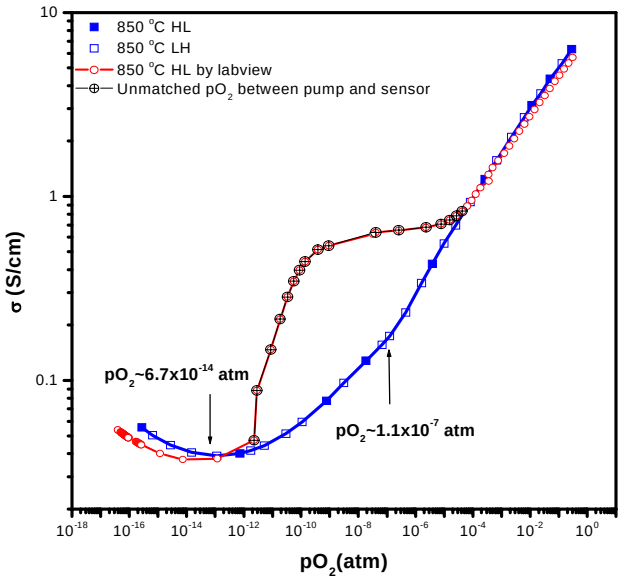

Figure 14. Comparison of two different sets of conductivity data measured for $La_{0.2}Sr_{0.8}Fe_{0.55}Ti_{0.45}O_{3-x}$ at 850 °C with different criteria for attainment of equilibrium.

Slow kinetics observed in dilatometry measurements:

The stoichiometry and thermal expansion data for $La_{0.2}Sr_{0.8}Fe_{0.55}Ti_{0.45}O_{3-\delta}$ are shown in Figure 15. At 790 °C, a linear relation between the chemical expansion and stoichiometry is observed. At

higher temperatures deviations become more pronounced and increase with increasing temperature. The chemical expansion initially increases faster and then plateaus at a lower pO_2 than would be predicted by the stoichiometry. The non equilibrium behavior observed in the chemical expansion data parallels that observed in the conductivity and suggests the occurrence of microscopic phase segregation on reduction.

Micro-structural Studies:

Samples of $La_{0.2}Sr_{0.8}Fe_{0.55}Ti_{0.45}O_{3-\delta}$ were quenched in air from 900 °C and different oxygen partial pressures $pO_2 = \sim 1.3 \times 10^{-4}$, 1.1×10^{-7}, 1.2×10^{-10}, 6.7×10^{-14} atm. All peaks in the X-ray powder diffraction patterns of the air quenched and non-quenched samples were indexed as corresponding to a cubic perovskite. No evidence is found of a phase transition in the whole region of pO_2 though the lattice parameter increases with the degree of reduction as expected.

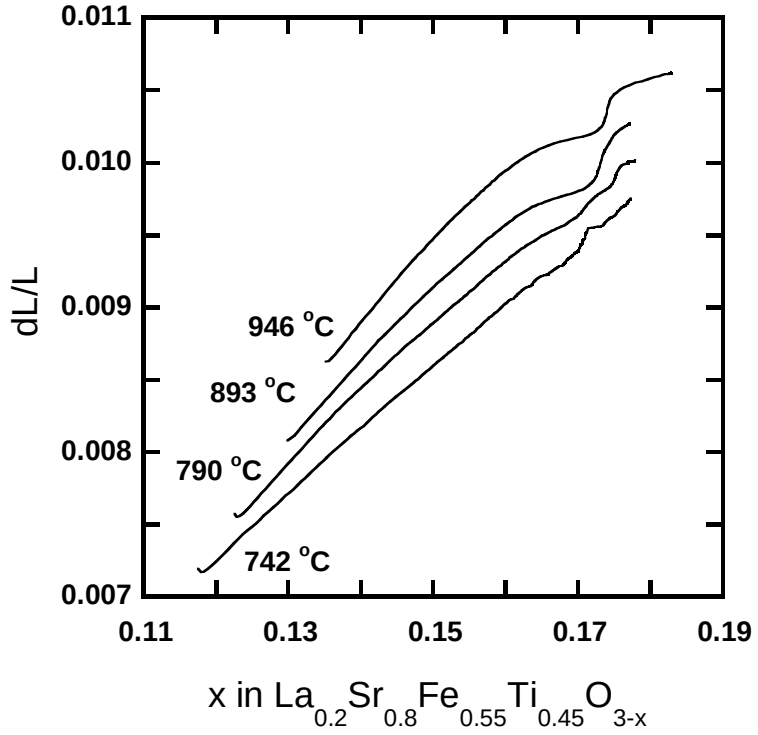

Figure 15. The dependence of the chemical expansion on non - stoichiometry in $La_{0.2}Sr_{0.8}Fe_{0.55}Ti_{0.45}O_{3-x}$ (from reference vii).

Two samples were examined by transmission electron microscopy (#2, #5). For sample #2 TEM observations indicate that there are two kinds of crystal grains existing in the sample. The major phase in the sample has well-crystallized cubic $La_{0.2}Sr_{0.8}Fe_{0.55}Ti_{0.45}O_{3-\delta}$ grains (about 90 %) (Figure 16a) but a small number of grains (10%) are of the cubic matrix containing pure Fe nanoparticles and a Fe-rich amorphous phase.

The compositions of the amorphous regions were determined by X-ray analysis and the iron nano particles by analysis of the lattice fringes. The iron nanoparticles were ~ 5nm in size The Moiré fringe covered areas in Figure 16c are Fe nano-particles overlapped with the cubic LSFTO crystal matrix. TEM observation of sample #5 also showed two distinct microstructures, one corresponding to well-crystallized cubic LSFTO (about 90 % of the whole sample) and the second area (~ 10%) containing an amorphous phase with a higher Fe concentration. No nanoparticles were observed in this sample.

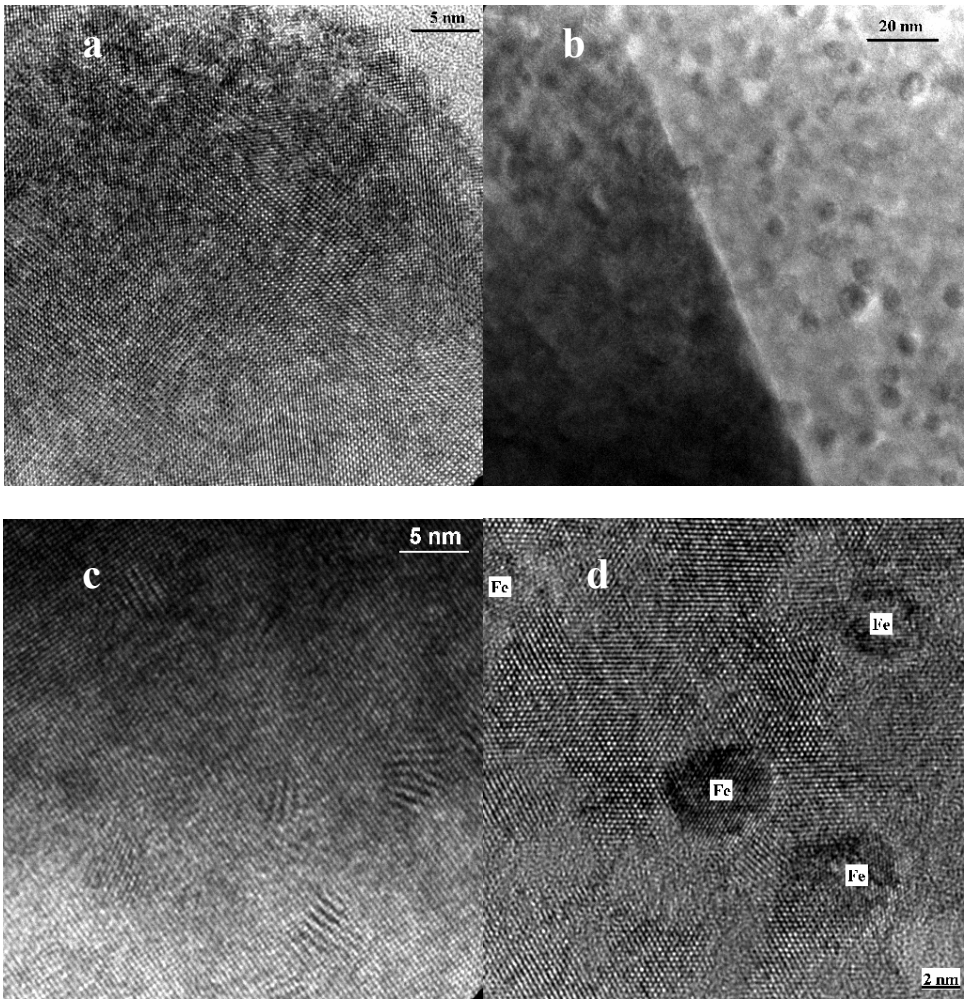

Figure 16. (a) a high resolution image of a defect free LSFTO grain, (b-d) three different magnifications a grain showing the presence of Fe nanoparticles and amorphous iron rich regions.LaSrFeTiO Bulk Sample 0285545#2

Comparison with LSFO

The reduction behavior of LSFTO is complex because of the number of components and the large number of possible decomposition pathways. The compound $La_{0.5}Sr_{0.5}FeO_3$ is simpler but shows the same general behavior in the conductivity on reduction [6]. A preliminary study of the reduction behavior in hydrogen indicated that the reduction was slow. After 24 h of treatment in flowing 5% H_2 at 950 °C, the X-ray diffraction data indicated partial decomposition to a mixture of the perovskite phase, $LaSrFeO_4$ and Fe as shown in Figure 16. After a further 24 h under the same conditions, the X-ray data indicate complete decomposition. It is interesting to note that similar results have been obtained in the deposition of perovskite thin films by pulsed laser deposition using a target of composition $La_{0.5}Sr_{0.5}FeO_3$ [3]. Under oxidizing conditions the films had the perovskite structure but under reducing conditions were found to contain iron nanowires and $LaSrFeO_4$.

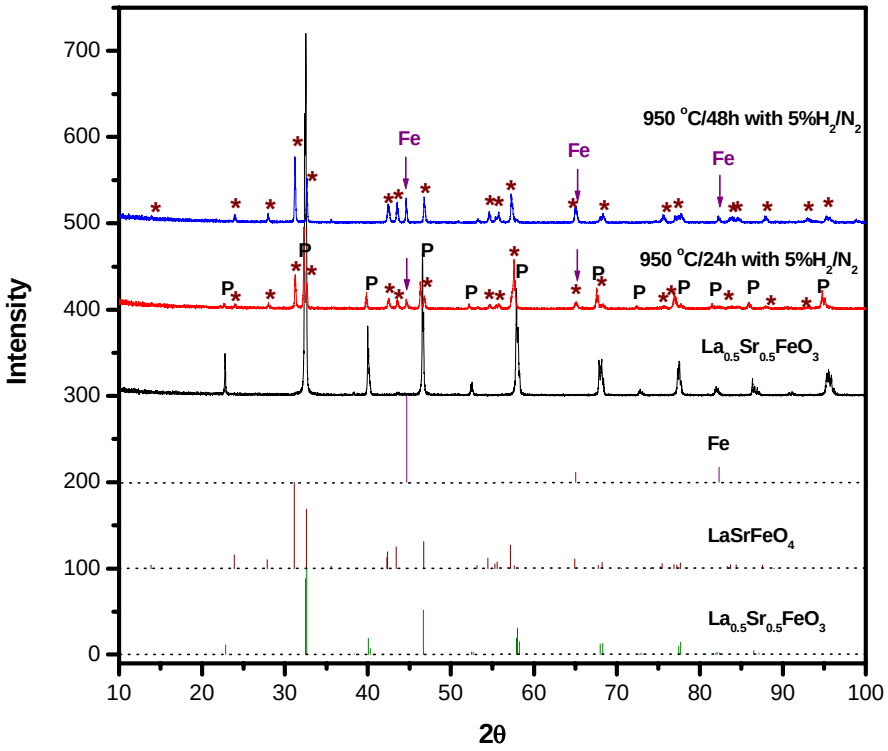

Figure 17. Powder X-ray diffraction spectra of $La_{0.5}Sr_{0.5}FeO_{3-\delta}$ and the reduction products together with reference spectra.

General Comments

The reduction behavior for LSFTO and LSFO is complex and proceeds with the introduction secondary phases. Cation rearrangements are responsible for the slow kinetic behavior. What is less clear is whether for a given set of reaction conditions, the behavior represents a slow approach to equilibrium or the formation of a metastable intermediate. In other systems, both kinds of behavior are observed. For example, in the reduction-$SrFeO_{3-x}$ at a temperature and pO_2 in the two phase region equilibrium is slow because of the kinetics of nucleation and growth of the brownmillerite structure [3] The reduction behavior of $LaCoO_3$ was investigated by reaction with zirconium metal in sealed tubes at 400°C. Two discrete vacancy ordered phases were observed, with compositions namely $LaCoO_{2.5}$ and $LaCoO_{2.67}$; $LaCoO_{2.5}$ reoxidizes via $LaCoO_{2.67}$ to $LaCoO_3$. Both oxygen deficient phases are metastable, and undergo irreversible decomposition to CoO and the Ruddlesden–Popper type phases La_2CoO_4 and $La_3Co_3O_{10}$ when heated above 650 °C in an inert atmosphere [3]

Considering all of the experimental data, the preferred kinetic pathway to reduction when the vacancy concentration corresponds to the formation of significant concentrations of Fe^{2+} is via the formation of a Ruddlesden –Popper phases as indicated below for the reduction of $La_{0.5}Sr_{0.5}FeO_{2.75}$.

$$La_{0.5}Sr_{0.5}FeO_{2.75} \rightarrow La_{0.5}Sr_{0.5}FeO_{2.75-\delta} \rightarrow (1-\delta/3)La_{0.5}Sr_{0.5}FeO_{2.75-\delta} + \delta/3LaSrFeO_4 + \delta/3Fe$$

Microscopically this may be viewed as beginning with the introduction of a planar defect as shown in the scheme below. Such defects have been observed in partially reduced $(La,Sr)FeO_{3-x}$ by high resolution electron microscopy [3.

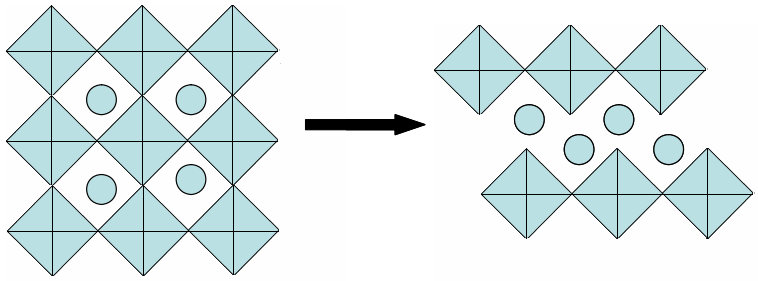

In the more complex composition, LSFTO, iron or iron rich phases are observed locally but we have found no evidence for the existence of presence of a Ruddlesden – Popper phase.

Finally, we note that both in stoichiometry and conductivity measurements in sealed cells, long equilibration times lead to equilibrium in the sense that measurements on increasing and

decreasing pO_2 agree, indicating that at least under these conditions phase separation on reduction is kinetically and not thermodynamically controlled.

Isotope transient studies

Table 2 shows the operating conditions, oxygen flux and kinetic parameters derived from the isotope transients for the tubular $La_{0.2}Sr_{0.8}Fe_{0.8}Cr_{0.2}O_{3-x}$ membrane operating at 1173 K under a high chemical gradient. The membrane and reactor assembly were leak-free, as determined by the lack of Ar permeation to the syngas side. The membrane showed two operating steady state conditions at 1173K: (1) a low flux, low gradient condition where oxygen evolution was observed on the "syngas" side along with CO and CO_2, and (2) a high flux, high gradient condition where only CO and CO_2 were observed on the syngas" side. A full description of this multiple steady-state behavior can be found elsewhere. The isotope

Table 2: $La_{0.2}Sr_{0.8}Fe_{0.8}Cr_{0.2}O_{3-x}$ membrane operating conditions and transport parameters from isotopic transient experiment. See text for details.

Temperature	1173K
Air side composition (1 atm) [a]	14 mol% O_2 : 86 mol% Ar
Syngas side composition (1 atm) [a]	21mol% CO : 29% mol% CO_2 : 50 mol% He
Oxygen flux (as O_2)	2.54 STD cm^3 min^{-1} cm^2 (sccm)
$k_{O,f}$ (both surfaces)	8.1×10^{-5} cm s^{-1}
D_O (average)	7.3×10^{-7} cm^2 s^{-1}
Reversibility at air side [b]	< 10%
Reversibility at syngas side [c]	< 10%
* outlet compositions	

[a] outlet conditions, feed conditions air side 20% oxygen, syngas side 45% CO, 5% CO_2.
[b] from ^{18}O content in O_2 after pulse
[c] from ^{18}O content in CO

Figure 18 shows the isotopic transient in the gas phase on the syngas side of the membrane at the conditions listed in Table 2. Most of the isotope appears in CO_2 (solid points) as the result of the oxidation of CO at the membrane surface, incorporating the delivered ^{18}O as it arrives. It was previously shown in IEDP measurements in CO_2:CO mixtures that oxygen scrambling between carbon dioxide and $La_{0.2}Sr_{0.8}Fe_{0.8}Cr_{0.2}O_{3-x}$ is extremely rapid under these conditions. Thus, the CO_2 isotopic composition and the membrane surface are the same throughout this transient experiment. Carbon monoxide can obtain ^{18}O atoms either by (1) exchange with the surface, or through the reverse of the CO oxidation reaction, i.e. the reduction of (labeled) CO_2. Under the chemical equilibrium conditions in the IEDP experiments, the forward and reverse rates of CO oxidation (CO_2 reduction) were equal. The small amount of ^{18}O in carbon monoxide in Figure 18

shows that the CO_2 reduction rate is less than 10% of the CO oxidation rate under the operating gradient in these experiments.

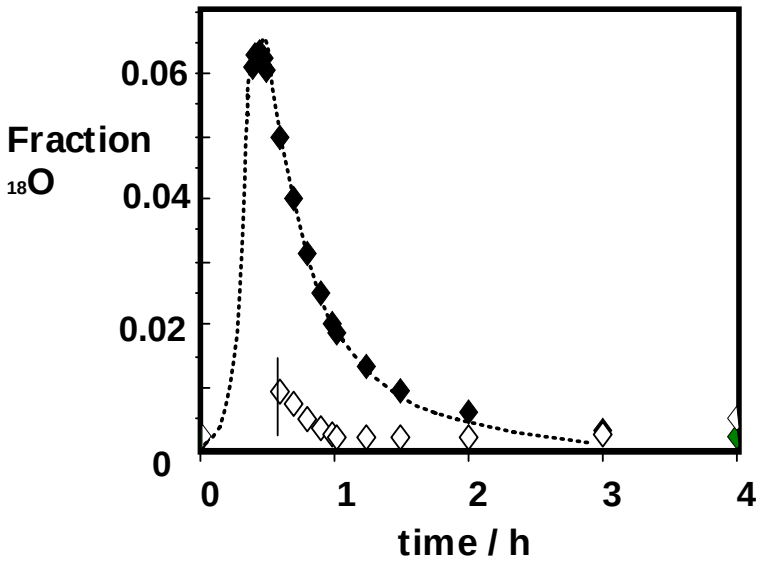

Figure 18: Isotope transient (fraction ^{18}O) in CO_2 (solid points) and CO (open points) at the membrane operating conditions in Table 1. The vertical line shows the high estimated uncertainty in the CO measurement due to high background.

The dashed line is the result of a one dimensional model simulation, described in full elsewhere. Briefly, the air side surface reaction is assumed to be partly reversible with $k'_{O,f}$ and $k'_{O,r}$ being the forward and reverse oxygen atom exchange rates respectively. The oxygen motion in the bulk is given by a combination of a flux term, Φ_O, and a diffusivity, D_O. Finally, the syngas surface processes are simulated by a forward and reverse CO oxidation rates, $k''_{CO,f}$ and $k''_{CO,r}$ with the CO_2 isotopic composition held equal to the syngas surface value to mimic the rapid scrambling process mentioned above. Both gas phases are assumed both assumed to be well-mixed, an approximation justified by consideration of the calculated gas phase diffusivities and the nominal gas residence time in the membrane region of the reactor. These kinetics parameters are held constant, including an assumption of a constant value of DO across the membrane (but see below). The resulting isotope balance equations are used to simulate the ^{18}O distribution with time and the parameters varied until a good fit to the data is obtained. The derived parameters are given in Table 2. Both surface reactions are essentially irreversible. In addition the chemical gradient and/or induced phase stabilities have a dramatic effect on the surface rates when compared to those in a low gradient situation (air separation or IEDP). Comparison with such low-gradient measurements on this material show a factor of three increase in $k'_{O,f}$ (air side). The CO oxidation rate ($k''_{CO,f}$) is approximately 20 times that on the oxidized surface and over a factor

ten higher than the CO oxidation rate measured in IEDP in reducing atmospheres. Almost nothing is known regarding the variation of the equilibrium surface composition, including oxygen defect density, of any complex oxide as a function of gas composition. Therefore the role of non-equilibrium phase segregation processes cannot be demonstrated conclusively here. However, the substantially higher rates of CO oxidation in this instance than in chemically equilibrated IEDP measurements at similar gas oxygen potential is suggestive of such involvement.

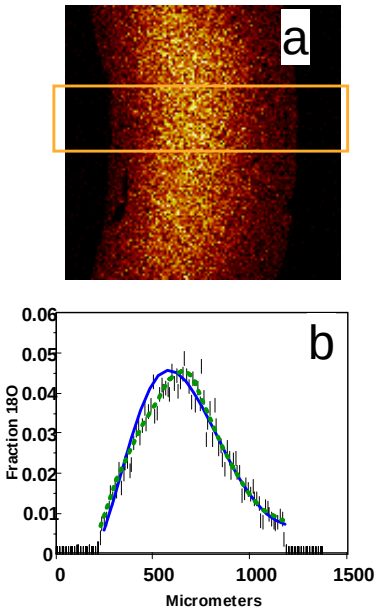

Figure 19. ^{18}O isotope distribution in a tubular membrane quenched during in isotopic transient. Panel (a) - ^{18}O ToF-SIMS image of a polished radial cross section. Panel (b) - ^{18}O radial profile from boxed region in panel a: vertical lines are the experimental ^{18}O fractions (height = ± 1 esd), solid line is the model fit with constant $D_O = 7 \times 10^{-7}$ cm^2 s^{-1}, dashed line is best model fit with a linear increase in D_O across the membrane (2 - 10 x 10^{-7} cm^2 s^{-1}).

The membrane was sacrificed during a repeat of the experiment in Table 1, with a somewhat shorter $^{18}O_2$ pulse. The membrane was quenched after rapid cooling 15 minutes after the isotope pulse had been administered. The resulting ^{18}O distribution of the polished radial cross-section is shown in Figure 7, both as a map (panel a) and as a profile (panel b). Other cross sections showed the profile to be largely invariant with axial and radial position. Two simulations of the internal profile are shown in panel b of Figure 7. One was obtained while assuming a constant value of D_O in the bulk, while the other assumed a linear variation of the diffusivity from 2 x 10^{-7} to 1 x 10^{-6} cm^2 s^{-1} as the radial position is varied from the air side to the syngas side. The shape of the internal isotope "wave" is clearly influenced by such variations, while the gas phase

transients are unaffected. Thus, it is necessary to obtain the internal isotope distribution in order to investigate the changes in bulk mobility under a chemical gradient. The result in Figure 7 does not show any evidence of a marked minimum in diffusivity which could occur if the mobility dropped drastically at one radial position because of reversible or irreversible changes in structure. The results are consistent with the measured equilibrium variability of the oxygen vacancy density and previous IEDP measurements.

CONCLUSIONS

The *in situ* electrical conductivity and Seebeck coefficient measurements were made on LSFT at 1000 and 1200°C over the oxygen activity range from air to 10^{-15} atm. The electrical conductivity measurements exhibited a p to n type transition at an oxygen activity of $1x10^{-10}$ at 1000°C and $1x10^{-6}$ at 1200°C. The magnitude of the electrical conductivity and position of the p to n transition is determined by both the relative concentrations of the electronic carriers as well as the oxygen vacancy concentration. Thermogravimetric studies were also carried out over the same oxygen activities and temperatures. According to the TGA study, the weight decreased continuously until dissociation occurred at 10^{-15} atm. Upon reoxidation, the weight loss was found to be reversible, eventhough, dissociation had occurred and the electrical conductivity had changed from p to n type. . This is a very good sign since LSFT not only exhibits higher conductivity (n-type) in the low oxygen activity regime, but also has a higher concentration of oxygen vacancies which improves the performance as an oxygen permeable membrane.

The LSFT and dual phase membranes were heat treated at 1000°C for 60min and air and N_2 atmosphere. The Fracture toughness and hardness of the heat treated membranes were calculated using Vicker's indentation method. The structural changes caused by the atmosphere have to be analyzed using x-ray diffraction and SEM. The membranes that are exposed to high temperatures at an inert and a reactive atmosphere undergo many structural and chemical changes which affect the mechanical properties. A complete transformation of fracture behavior was observed in the N_2 treated LSFT samples.

Considering all of the experimental data, one preferred kinetic pathway to reduction of perovskite ferrites when the vacancy concentration corresponds to the formation of significant concentrations of Fe^{2+} is via the formation of a Ruddlesden –Popper phases. In more complex compositions, such as LSFTO, iron or iron rich phases are observed locally with no evidence for the existence of presence of a Ruddlesden – Popper phase. In both stoichiometry and conductivity measurements in sealed cells, long equilibration times lead to equilibrium in the sense that measurements on increasing and decreasing pO_2 agree, indicating that at least under these conditions phase separation on reduction is kinetically and not thermodynamically controlled.

The combination of gradientless measurements with isotope investigations under steady state, provide a complete picture of the performance of OTM materials. In the case of the $La_{0.2}Sr_{0.8}Fe_{0.8}Cr_{0.2}O_{3-x}$ membrane here, the irregular structural changes observed in these materials are implicated in the large variation in observed surface rates.

REFERENCES:

1. H. J. M. Bouwmeester, A. J. Burggraaf, "*The CRC Handbook of Solid State Electrochemistry*", Eds. P. J. Gellings and H. J. M. Bouwmeester, CRC Press, Boca Raton, (1997) 481.
2. J. Yoo, A. Verma, and A. J. Jacobson, Proc. Electrochem. Soc. PV2001-28 (2002) 27.
3. J. Yoo, A. Verma, S. Wang, and A. J. Jacobson, J. Electrochem. Soc. 152 (2005) A497.
4. C.Y. Park and A. J. Jacobson, J. Electrochem. Soc. 152 (2005) J65.
5. C. Y. Park and A. J. Jacobson, Solid State Ionics 176/35-36 (2005) 2671.
6. J. Yoo, C. Y. Park and A. J. Jacobson, Solid State Ionics 175(1-4) (2004) 55.
7. V. L. Kozhevnikov, I. A. Leonidov, M. V. Patrakeev, E. B. Mitberg, and K. R. Poeppelmeier, J. Solid State Chem. 158 (2001) 320.
8. I. A. Leonidov, V. L. Kozhevnikov, M. V. Patrakeev, E. B. Mitberg, and K. R. Poeppelmeier, Solid State Ionics 144 (2001) 361.
9. M. V. Patrakeev, J. A. Bahteeva, E. B. Mitberg, I. A. Leonidov, V. L. Kozhevnikov, and K. R. Poeppelmeier, J. Solid State Chem. 172 (2003) 219.
10. M. V. Patrakeev, I. A. Leonidov, V. L. Kozhevnikov, K. R. Poeppelmeier, J. Solid State Chem. 178 (2005) 921.
11. V. L. Kozhevnikov, I. A. Leonidov, J. A. Bahteeva, M. V. Patrakeev, E. B. Mitberg, and K. R. Poeppelmeier, Chem. Mater. 16 (2004) 5014.
12. E. V. Tsipis, M. V. Patrakeev, V. V. Kharton, A. A. Yaremchenko, G. C. Mather, A. L. Shaula, I. A. Leonidov, V. L. Kozhevnikov, and J. R. Frade, Solid State Sciences 7 (2005) 355.
13. L. Mohaddes-Ardabili, H. Zheng, S. B. Ogale, B. Hannoyer, W. Tian, J. Wang, S. E. Lofland, S. R. Shinde, T. Zhao, Y. Jia, L. Salamanca-Riba, D. G. Schlom, M. Wuttig, and R. Ramesh, Nature Materials 3 (2004) 533.
14. L. M. Liu, T. H. Lee, L.Qiu, Y.L. Yang, and A.J. Jacobson, Mater. Res. Bull., 31 (1996) 29.
15. O. H. Hansteen, H. Fjellvåg and B. C. Hauback, J. Mater. Chem. 8 (1998) 2081.
16. R. F. Klie and N. D. Browing, Microsc. Microanal. 8 (2002) 475.

BIBLIOGRAPHY **N/A**

LIST OF ACRONYMS AND ABBREVIATIONS

YSZ	Yttria stabilized zirconia
XRD	X-ray diffraction
$La_{0.2}Sr_{0.8}Fe_{0.55}Ti_{0.45}O_{3-\delta}$	LSFTO
IEDP	Isotope exchange and depth profiling
SIMS	Secondary Ion Mass Spectroscopy